Computer simulation of thermal modelling of alkaline hydrogen/oxygen fuel cells

A. Baumann, S. Hauff and **K. Bolwin***
German Aerospace Research Establishment (DLR), Institute for Technical Thermodynamics, 7000 Stuttgart 80 (F.R.G.)

(Received March 12, 1991; in revised form May 20, 1991)

Abstract

An essential problem connected with the operation of regenerative fuel cell systems in space is the rejection of waste heat, produced mainly during discharging the regenerative fuel cell. The intention of this investigation was to gain a better understanding of the heat generation and heat rejection mechanism in alkaline fuel cells by performing detailed thermal modelling of a single cell stack. In particular, spatial temperature profiles within the fuel cell stack and the start-up behavior of the cells were predicted. Furthermore a model simulation of an emergency situation due to a partial failure of the coolant circuit was performed and theoretically temperature versus time curves were given for restarting the cooling.

Introduction

Interconnection of fuel cell and electrolyzer is a favourable approach to reduce the expense of in-orbit installation and fuel replacement of energy supply systems for future long term space missions. Recently it was shown, that regenerative fuel cell (RFC) systems for space application have a distinct advantage regarding the design layout compared with state of the art battery systems [1–3]. An additional advantage arises from the capability of integrating the media supply of both environmental control and life support (ECLS) and propulsion purposes.

The present investigation is a comprehension of our recent work on a simple one-dimensional model to predict the spatial and time dependent temperature profiles in alkaline fuel cells designed in the VARTA Eloflux concept [4–7].

The performed calculations consider the effects of the internal, non-linear, temperature dependent heat conductivity and thermal capacity. The coefficients of the heat transfer from the structure materials to the cooling medium have been calculated considering the velocity of the coolant flow and the cross-section of the flow drain. In addition we calculated the amount of heat generation assuming the temperature dependent characteristic of the

*Author to whom correspondence should be addressed.

0378-7753/91/$3.50

fuel cell. The amount of waste heat generated in the different structural elements of the cell is directly related to the ohmic and polarization losses in these components.

Waste heat rejection is assumed due to free convection across the surface of outer cooling coils. The geometry of these cooling coils is not changed during performing the simulation, thereby the cooling capability is influenced by the temperature difference from coolant to ambiency only.

Model simulation has been performed to gain more information regarding the following questions:

- the temperature distribution during starting up fuel cell operation
- the temperature distribution during stationary operation
- the entire amount of generated and rejected waste heat during start-up operation
- critical time constants regarding malfunction of the cooling system

Knowledge of these topics is essential in developing an optimized thermal management for regenerative fuel cells.

Description of the thermal modelling

To perform system analysis, a detailed understanding of the fuel cell arrangement and operation is necessary. Since a detailed description of the method of operation and the construction of a fuel cell designed in the Eloflux principle is given elsewhere [4–7], in this work only a brief outline of the design and the properties of the structural elements are given .

The particular property of the alkaline Eloflux fuel cell is the electrolyte flow that moves perpendicularly to the electrode surface across the cell stack. This flow is possible due to the highly porous structure and the compact arrangement of all constructive elements. The Eloflux flow supports the removal of the produced water from the reaction sites and supplies the fuel cell reaction with electrolyte.

The fuel cell is designed as a stack of different thin layers (e.g. electrodes, separators and electrolyte distributors), containing all structural elements for reactant and coolant supply and rejection. A single cell consists of four pairs of hydrogen and oxygen electrodes. The electrodes are separated by insulating layers (e.g. asbestos) from each other. The electrolyte distributors on the transversal plane of the cell should distribute the electrolyte flow into the Eloflux and a bypass flow (Fig. 1). Heat generation occurs mainly on the electrode layers, whereas heat transfer to the coolant occurs in the electrolyte distributors. Note that the Eloflux flow should support the kinetic of the reactant transport, whereas the excess electrolyte flow is responsible for the waste heat rejection.

For thermal modelling the fuel cell is spaced into fifteen volume elements, reasonably these elements are directly related to the structural elements of the cell. Calculation was performed on the basis of the following assumptions.

- There is no spatial temperature distribution in a single volume element.

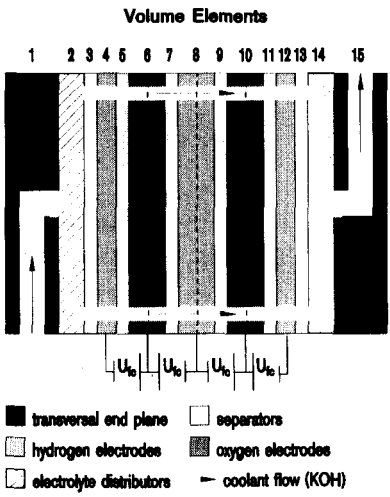

Fig. 1. Scheme of the Eloflux fuel cell, consisting of fifteen structural elements.

- Heat exchange between the surface of the block and the ambiency is negligible, the cell is perfectly isolated.
- The specific heat capacity is assumed to be temperature dependent.
- Waste heat generation is directly related to the cell characteristics. Polarization on both the oxygen and hydrogen electrodes is responsible for fractional losses of 75% and 15%, respectively. These values are related to the overpotentials which are known from electrochemical investigations on these electrodes. In addition 10% of the waste heat is produced due to the ohmic losses in the electrolyte volume. This is deduced from the Tafel slope, assuming reasonable current densities.
- The enthalpy flow within the exhaust gas due to incomplete fuel conversion or purging rates does not contribute significantly to the cell cooling.
- The thermal flow across the boundary of the structural elements is related to the heat transport mechanism in the electrolyte: since the structural elements of the considered fuel cell design are highly porous, the junction between neighbouring elements is assumed to be small.
- Since we have made no assumptions about the removal process of the produced water, the contribution of this process to the entire thermal balance has to be neglected. In this first approach, the required energy $\Delta E = 42.5$ kJ/mol is related to external sources.

Since the temperature of a certain element is determined by both the heat transfer across the boundary to the next volume and heat generation inside the considered volume, the calculation is based on the energy conservation principle expressed in the form of the continuity equation.

$$\frac{\mathrm{d}}{\mathrm{d}t} Q = \oint \dot{q}(t) \mathrm{d}A + \frac{\partial Q}{\partial t} \tag{1}$$

where Q denotes the heat temporary contained in the volume and $\dot{q}$ denotes

the heat flow density across the boundary of the considered volume. Since the heat content itself is related to the temperature via the heat capacity and the mass of the element, the left side of eqn. (1) can be expressed as:

$$\frac{dQ}{dt} = \frac{\partial Q}{\partial m}\frac{dm}{dt} + \frac{\partial Q}{\partial c}\frac{dc_p}{dt} + \frac{\partial Q}{\partial T}\frac{T}{dt} \tag{2}$$

Here m and c_p denote the mass and the heat capacity, respectively. Assuming time independent mass and heat capacity of the elements, eqn. (2) simplifies to

$$\frac{dQ}{dt} = m \times c_p \times \frac{dT}{dt} \tag{3}$$

The first term on the right side of eqn. (1) describes the thermal transfer across the boundaries of the desired volume. We have to consider two contributions to the entire heat transfer: thermal conduction and the thermal flow of the coolant. The heat conduction is determined by the heat conductivity λ, the area A across which the heat is transferred and the gradient of the temperature dT/dx.

This relation is described by Fourier's equation:

$$Q_{con} = -\lambda(T) \times A \times t \times \frac{dT}{dx} \tag{4}$$

Since λ is temperature dependent, the heat conductivity of water is approximated by a polynome of second order in the temperature range between 290 and 370 K. Calculation of λ_{KOH} is made considering a decrease of 5.6% regarding the heat conductivity of water [8].

$$\lambda_{KOH}(T) = -0.437 + 5.57 \times 10^{-3} T - 6.88 \times 10^{-6} T^2 \tag{5}$$

In addition to thermal conduction, the contribution of the coolant flow to the entire heat transfer has to be considered. The thermal flow of the coolant can be described by eqn. (6)

$$\dot{Q}_{flow} = \dot{m}H + \dot{m}(e_{kin} + e_{pot}) + \dot{W}_t \tag{6}$$

where H and W_t denote the enthalpy and the technical work, respectively. Since the kinetic energy of the coolant flow e_{kin} is negligible compared to the enthalpy, and both the potential energy and the technical work do not contribute to the heat transfer in the fuel cell, the thermal flow is reduced to the enthalpy flow:

$$\dot{Q}_{flow} = \dot{m}H \tag{7}$$

Using the relation $H = c_p(T)T$, the entire heat transfer can be expressed by

$$\dot{Q} = \dot{Q}_{con} + \dot{Q}_{flow}$$

$$= -\lambda(T) \times A \times \frac{dT}{dx} + \dot{m} \times c_p(T) \times T \tag{8}$$

The second term on the right side of eqn. (1) denotes the waste heat generation inside the desired volume during operation of the fuel cell. In general, the amount of heat from the electrochemical reaction is given by the product of the polarization voltage and the discharge current. In addition we have to consider the heat generated due to entropy changes during the chemical reaction: $\Delta H = \Delta G + T\Delta S$. Taking these contributions into account we refer the thermodynamic losses of the reaction to the thermoneutral voltage U_0, which is related to the gross calorific value ΔH.

The heat generation is calculated on the basis of a fit to the experimental cell characteristics. The temperature dependent characteristic as described by eqn. (9) coincides sufficiently with the experimental data:

$$U_{fc} = 1 - (1.75 - 1.25 \times 10^{-2}(T - 293.15))i \tag{9}$$

where U_{fc} and i denote the cell voltage and the current density, respectively. Subsequently the heat generation is obtained from the difference between cell voltage and the thermoneutral voltage U_0:

$$\partial Q/\partial t = -z \times F(U_0 - U_{fc}(T, i)) \tag{10}$$

where z denotes the valence of the ions, which are responsible for the charge transfer in the electrochemical reaction and F is Faradays constant.

The temperature behavior of the fuel cell can be expressed by substitution of eqns. (3) and (8) into eqn. (1) and subsequent integration. The different KOH flows in an Eloflux fuel cell, e.g. the Eloflux and the coolant flow, are taken into account by summation over the parameter j. T_j denotes the temperature belonging to the flow.

$$T = \int \frac{\lambda(T) \times A \times \dfrac{dT}{dx} + \sum \dot{m}_j \times c_{p,j}(T_j) \times T_j + \dfrac{\partial Q}{\partial t}}{\sum m_j c_{p,j}} \, dt \tag{11}$$

The T_j are not *a priori* equal to the temperature of the structure. However, since the Eloflux flow is very slow, i.e. 1 ml/h, this temperature is assumed to be equal to the structure temperature: $T_{ELO} = T$. On the other hand, the coolant temperature T_{cool} depends on the waste heat generation of the fuel cell and waste heat rejection in outer cooling coils. The amount of heat rejection and the input temperature T_{in} of the coolant are determined from the temperature at the coolant output T_{out} assuming free convection across the surfaces of the cooling coils. Consideration of these relations demands knowledge about the heat transition from the outer cooling coils to air. Additionally, the heat rejection is mainly influenced by the heat transition from the structural material to the coolant (e.g. KOH), since the thermal flow is conducted through the coolant drains to the cooling coils. Depending on the operating state of the fuel cell, the flow can be both laminar and turbulent. With regard to the critical Reynolds number of 2320, this behavior results in different Nusselt relations.

First we consider the laminar flow. Assuming a coincident hydrodynamic and thermal input, it was found [9] that

$$\mathrm{Nu}=\frac{\alpha(T)d}{\lambda(T)}=\left[3.66+\frac{0.0677\left(\mathrm{Pe}\,\frac{d}{l}\right)^{1.33}}{1+0.1\left(\mathrm{Pe}\,\frac{d}{l}\right)^{0.83}\left(\frac{\mathrm{Pe}}{\mathrm{Re}}\right)^{0.17}}\right] \tag{12}$$

where α denotes the heat transition coefficient and d denotes the diameter of the coolant drain. $\mathrm{Pe}=w\cdot d/a$ and $\mathrm{Re}=w\cdot d/v$ denote the Péclet and Reynolds number, respectively. From eqn. (12) the heat transition coefficients are deduced:

$$\alpha(T)=\frac{\lambda(T)}{d}\left[3.66+\frac{0.0677\left(\frac{wd}{a(T)}\times\frac{d}{l}\right)^{1.33}}{1+0.1\left(\frac{wd}{a(T)}\times\frac{d}{l}\right)^{0.83}\left(\frac{v}{a(T)}\right)^{0.17}}\right] \tag{13}$$

where w denotes the velocity of the coolant flow and v is the kinematic viscosity. The coefficient a is defined as: $a=\lambda/\rho c_p$. From eqn. (5) and the material data we deduce: $a_{\mathrm{KOH}}=2.7\times10^{-7}\cdot\lambda_{\mathrm{KOH}}(T)$. From ref. 8 we deduce: $v_{\mathrm{KOH}}=1.3\times10^{-6}$ m^2/s. Finally we consider the turbulent flow. The Nusselt relation is given in ref. 9.

$$\mathrm{Nu}=\frac{\alpha(T)d}{\lambda(T)}=0.0235\left[\left(\frac{wd}{v}\right)^{0.8}-230\right]\times\left[1.8\left(\frac{v}{a(T)}\right)^{0.3}-0.8\right]\times\left[1+\left(\frac{d}{l}\right)^{2/3}\right] \tag{14}$$

From eqn. (14) we deduce for the heat transition coefficient:

$$\alpha(T)=\frac{\lambda(T)}{d}\times0.0235\times\mathrm{Nu} \tag{15}$$

To avoid a singularity for the transition from laminar to turbulent flow, the Nusselt relation is assumed to be linear when the Reynolds number is close to 2320. The heat transition to the coolant is now given by eqn. (16).

$$\dot{Q}_{trans}=\alpha(T)A\Delta T \tag{16}$$

where ΔT denotes the temperature which is responsible for the thermal transition and A is the surface of the coolant drain.

Considering the limiting conditions for the different volume elements, we can deduce the related heat transfer $\mathrm{d}Q_n/\mathrm{d}t$ and the temperature behavior $\mathrm{d}T_n/\mathrm{d}t$ from this theoretical framework. Since $T_{\mathrm{cool,n}}$ still depends on the temperature of the surrounding volume elements, it has to be calculated iteratively. The complete equations for all volume elements are given in ref. 10.

Finally let us consider the heat rejection from the outer cooling coils. From the energy conservation we deduce for the rejected heat flow $\mathrm{d}Q_r/\mathrm{d}t$:

$$\frac{dQ_r}{dt} = \frac{dQ_{out}}{dt} - \frac{dQ_{in}}{dt} \tag{17}$$

Simple arithmetic transformation using the relation $\dot{Q} = \dot{m} c_p T$ and insertion of eqn. (16) into eqn. (17) leads to an expression for the electrolyte temperature at the stack input:

$$T_{in} = \frac{T_{out} \times \dot{m}_{KOH} \times c_{p,KOH} + \alpha_{air} \times A_{coil} \times \left(T_{amb} - \frac{T_{out}}{2} \right)}{\dot{m}_{KOH} \times c_{p,KOH} + \frac{\alpha_{air} \times A_{coil}}{2}} \tag{18}$$

where T_{out} and T_{amb} denote the electrolyte temperature at the stack exit and the ambient temperature, respectively; α_{air} denotes the heat transition coefficient between the cooling coils with the surface A_{coil} and air, assuming free convection. From experimental data the product of α and A is set to: $\alpha_{air} A_{coil} = 0.83$ W/K.

This thermal modelling of the fuel cell leads to different types of relations. First we deduced algebraic expressions, considering the thermal transition from the volume elements to the coolant flow, which have to be solved iteratively. On the other hand, the temperatures of the volume elements are given by differential equations. Since the volume elements are interconnected by heat, fuel and coolant interchange, the differential equations are correlated to each other. From this, an analytical solution of the equations cannot be given, and the differential equations are solved numerically.

Results and discussion

Based on the described thermal modelling, spatial temperature profiles along the direction perpendicular to the electrode surfaces have been calculated. The limiting conditions due to the operation state of the fuel cell are given by the current density, which is related to the power via the cell characteristics and the coolant flow density. The rated power of the single cell stack, considered in the simulation of $P_r = 50$ W, is correlated to a current density of $i = 150$ mA/cm^2 via the total electrode area of $A_{El} = 400$ cm^2. Simulation has been performed assuming over load operation at $i = 250$ mA/cm^2 and rated load operation at $i = 150$ mA/cm^2. The coolant flow is varied from $\dot{m}_{cool} = 2$ l/h to $\dot{m}_{cool} = 10$ l/h. Simulation is started setting the temperature of both the cell stack and the coolant to ambient values (20 °C).

Figure 2 shows temperature profiles across the cell stack during the first phase of 60 s of start-up operation. The isochronous curves are spaced by a period of 2 s. The data are plotted versus the volume elements numbered from one to fifteen. In this presentation, the hydrogen electrodes are rep-

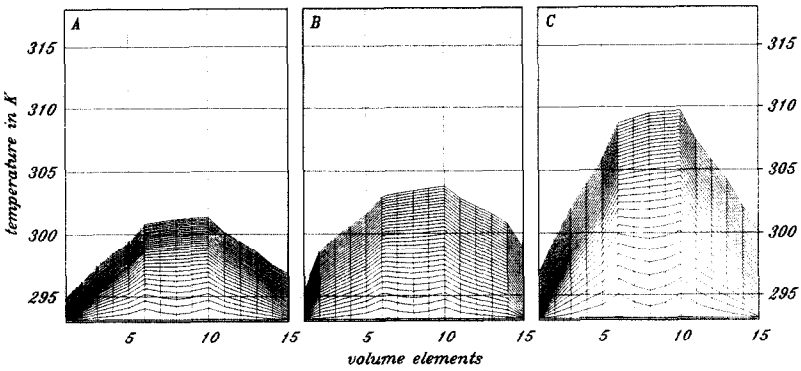

Fig. 2. Spatial temperature profiles across the cell stack during start-up operation. Calculations were performed assuming $i = 150$ mA/cm^2, $\dot{m}_{cool} = 10$ l/h (A); $i = 150$ mA/cm^2, $\dot{m}_{cool} = 2$ l/h (B); $i = 250$ mA/cm^2, $\dot{m}_{cool} = 10$ l/h (C).

resented by the volume elements four, eight and twelve, whereas the oxygen electrodes are represented by the volumes six and ten.

Reasonably the volume elements generating the largest amount of waste heat can be identified locating the maxima of the temperature profile when starting the operation. However a few seconds later the distinct profile is equalized due to heat conduction from the main heat sources to the cooler volume elements. The temperature profile shows a broad smooth plateau in the center of the fuel cell including the volume elements 6 to 10 and decreasing temperatures towards the transversal plane of the cell stack, indicating the location of the coolant flow. The appearance of the asymmetric shape of the profiles in calculations assuming very low coolant flow densities is explained by the direction of the coolant flow.

To obtain a better understanding of the time dependency of the thermal profiles, the temperatures of interesting volume elements are plotted versus time, as shown in Fig. 3. The selected volume elements are: both the transversal end planes (VE1, VE15), the electrolyte distributor at the electrolyte input (VE2) and both the hydrogen and oxygen twin electrodes (VE8, VE6).

The time dependency of the temperature in the selected volume elements show distinct characteristic details.

Immediately after starting the operation, the oxygen twin electrode shows the highest temperature gradient. This result is reasonable, since the waste heat generation is mainly located in this volume element. However a few seconds later, the temperature at the hydrogen twin electrode, located in the center of the cell stack, increases highly due to the heat conduction from the surrounding elements. Since the spatial temperature profile shows distinct asymmetry, the temperature of the hydrogen twin electrode exceeds the temperature of the oxygen twin electrode VE6, but not those of VE10 (see Fig. 1 for the notation of the volume elements).

In the volume element VE1 only a slight increase of the temperature is observable immediately after start-up operation, however changes in the

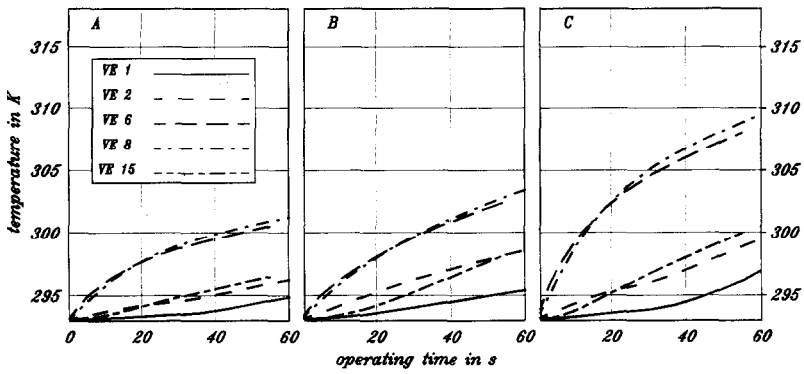

Fig. 3. Time dependent temperature behavior of selected structural elements during start-up operation. Calculations were performed assuming: $i = 150$ mA/cm^2, $\dot{m}_{cool} = 10$ l/h (A); $i = 150$ mA/cm^2, $\dot{m}_{cool} = 2$ l/h (B); $i = 250$ mA/cm^2, $\dot{m}_{cool} = 10$ l/h (C).

thermal management are indicated by the increased slope of the temperature characteristic after operating the fuel cell for more than 35 s. An explanation of this behavior is given by the limiting conditions of the outer cooling coils. The capacity of the assumed cooling coils is not able to cool the electrolyte down to ambient temperature. This leads to increasing coolant temperatures at the electrolyte input (VE1). While the temperature of VE1 is influenced during the first seconds after start-up operation by heat conduction only, an additional dependency from the coolant temperature is evident later. Since the temperature at the electrolyte exit (VE15) depends on its input temperature, a similar behavior is observed for the last volume element of the cell stack (VE15).

While the quantitative behavior of the shown temperature characteristics is not influence by the assumed load of the fuel cell – changes are only observable in the absolute level and the slopes of the temperature curves – the temperatures of the transversal planes regarding the temperature of the cell stack are distinctly influenced by the coolant flow density as indicated by the intersection of the temperatures of VE2 and VE15 (see Fig. 3).

Secondly the temperature distribution during stationary operation is examined. The maximal temperatures of the different volume elements during steady state operation should not exceed limiting values to avoid damage of the structural materials (e.g. electrodes or framework). Figure 4(A) shows spatial temperature profiles across the cell stack assuming a current density of $i = 150$ mA/cm^2 and a coolant flow density of $\dot{m}_{cool} = 10$ l/h; the profiles are spaced by 120 s. For the assumed parameters, the temperatures do not exceed 345 K after 3600 s operating time, and the temperature differences do not exceed 7.1 K.

A better graphical representation of the transition from start-up to equilibrium state of operation is given in the form of a temperature versus time plot (see Fig. 5). An asymptotic behavior of the temperatures is evident,

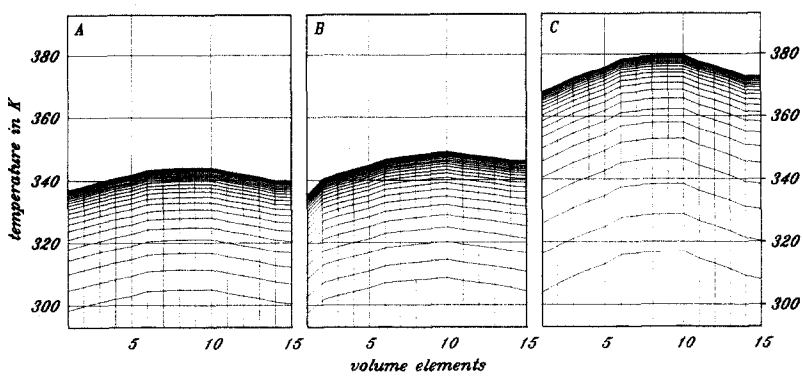

Fig. 4. Spatial temperature profiles across the cell stack showing the transition from the start-up phase to the equilibrium state. Calculations were performed assuming $i = 150$ mA/cm^2, $\dot{m}_{cool} = 10$ l/h (A); $i = 150$ mA/cm^2, $\dot{m}_{cool} = 2$ l/h (B); $i = 250$ mA/cm^2, $\dot{m}_{cool} = 10$ l/h (C).

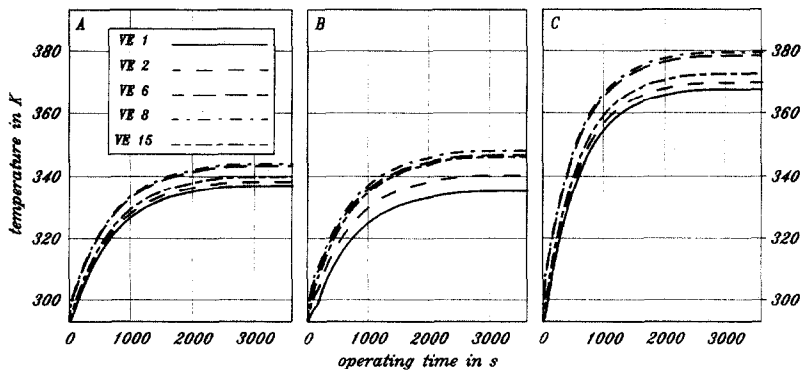

Fig. 5. Time dependent temperature behavior of selected structural elements showing the transition from the start-up phase to the equilibrium state. Calculations were performed assuming: $i = 150$ mA/cm^2, $\dot{m}_{cool} = 10$ l/h (A); $i = 150$ mA/cm^2, $\dot{m}_{cool} = 2$ l/h (B); $i = 250$ mA/cm^2, $\dot{m}_{cool} = 10$ l/h (C).

and the equilibrium state is reached independently from the limiting conditions (e.g. i, I_{cool}) after 2500 s of operation.

The equilibrium state temperatures of the volume elements are given in Table 1 depending on the operating parameters of the fuel cell. In general, increasing load factors as well as decreasing coolant flow lead to increasing temperatures. However the temperature of the coolant input (VE1) may show decreasing temperatures when the coolant flow decreases due to a more sufficient cooling.

During the transition from start-up to equilibrium operation, the amount of both waste heat generation and heat rejection varies due to their temperature dependency.

Since the convection across the cell surface is neglected in the present work, the total amount of heat generated from the fuel cell can be expressed

TABLE 1

Stationary temperatures of the fuel cell elements. All temperatures are given in °C for different operating conditions

Volume elements	$i = 150$ mA/cm^2 $\dot{m}_{cool} = 10$ l/h	$i = 150$ mA/cm^2 $\dot{m}_{cool} = 10$ l/h	$i = 250$ mA/cm^2 $\dot{m}_{cool} = 10$ l/h
VE1	63.8	62.1	94.5
VE2	65.1	67.2	96.7
VE3	66.5	68.9	99.1
VE4	67.6	70.3	100.9
VE5	68.7	71.6	102.7
VE6	70.2	73.5	105.2
VE7	70.5	74.2	105.8
VE8	70.8	74.9	106.3
VE9	70.9	75.5	106.4
VE10	70.9	75.8	106.4
VE11	69.7	75.0	104.5
VE12	68.9	74.5	103.1
VE13	68.0	73.9	101.6
VE14	66.8	73.1	99.6
VE15	66.8	73.0	99.5

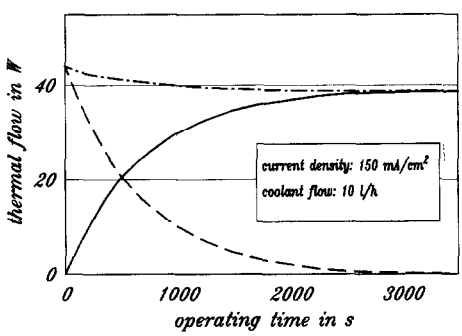

Fig. 6. Thermal flows of the generated waste heat, heat rejection and the heat stored sensibly within the fuel cell.

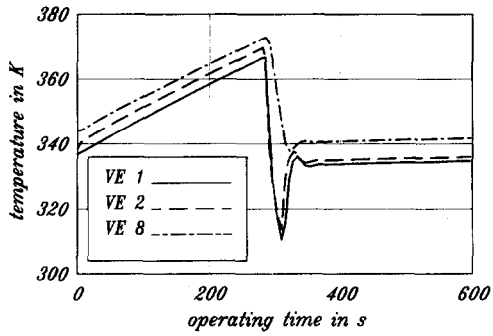

Fig. 7. Time dependency of the temperatures of selected fuel cell components during malfunction of the cooling system and readjustment of the equilibrium state after restarting the coolant flow.

by the sum of the heat dissipated by the coolant flow and the sensible heat stored within the fuel cell stack. In an equilibrium state of operation waste heat generation is balanced by the heat dissipation due to the cooling mechanism, while during the start-up an increasing cell temperature indicates that the heat is stored in the fuel cell.

In Figure 6 the time dependent rates of waste heat generation (dash dotted line) and heat rejection (solid line) are shown. The dash dotted curve is related to the temperature dependency of the fuel cell characteristics. The rate of waste heat stored sensibly in the fuel cell can be calculated from

the difference of the curves (dashed line). These data represent the mean value of the temperature gradient, averaged over the whole cell stack.

In agreement with the results discussed above, the equilibrium state is reached after 2500 s of operation. The rates of waste heat generation and rejection are equalized and the temperature gradient becomes zero. Note, that Fig. 6 describes the thermal behavior of the entire cell stack, not of a single volume element.

Finally we investigated the thermal behavior of the fuel cell during a malfunction of the cooling system. Our intention on performing this investigation was to obtain knowledge about critical time constants regarding emergency actions. These calculations were performed, setting the start values of the electrolyte and cell temperature to their equilibrium values obtained from previous calculations. The malfunction of the cooling system is simulated assuming a coolant flow of $\dot{m}_{cool} = 0$ l/h, fuel cell operation continuous, assuming an current density of $i = 150$ mA/cm^2. The continuing fuel cell operation results in a fast increase of the temperatures by $\Delta T = 30$ K in less than 300 s. Immediately decreasing temperatures are observed, assuming a restart of the coolant. The results of this calculation are shown in Fig. 7 for the hydrogen twin electrode (VE8), the transversal end planes of the cell stack (VE1) and the electrode distributor (VE2).

Whereas the volume elements serving for the thermal transition from the cell structure to the coolant show distinct oscillations of the temperature curve, the temperatures of the hydrogen twin electrode show extremely damped oscillations. The appearence of these reentry oscillations is predicted to take place within the first 70 s after restarting the coolant flow, followed by a monotone increase of the cell temperature, until the equilibrium state is reached after additional 1000 s. Although the equilibrium state is adjusted slowly, the temperatures differ from the equilibrium values by 3 K only, when the reentry oscillations are damped.

The distinct decrease of the temperatures of VE1 and VE2 below the equilibrium values is explained by the supply of cold electrolyte from the outer cooling coils to the volume elements resulting in a high efficient cooling of the fuel cell. The following oscillations are mainly influenced by the limiting conditions of the construction of the cooling coils. Hot electrolyte located within the cell stack during the malfunction is resupplied to the fuel cell, when the coolant flow has drifted through the cooling coils, leading to a more insufficient cooling.

The predicted temperature behavior of the hydrogen twin electrode is smoothed due to thermal conduction, since in the electrodes no heat transition to the coolant takes place.

From these calculations the critical time constants regarding the malfunction of the coolant circuit can be determined. Assuming a maximum temperature of 373 K (100 °C) for short time over load operation, the fuel cell has to switch off within the first 285 s after malfunction occurs. Restarting the coolant circuit leads to a readjustment of equilibrium temperatures within the next 60 s. Although reentry oscillation is predicted, no subcooling occurs

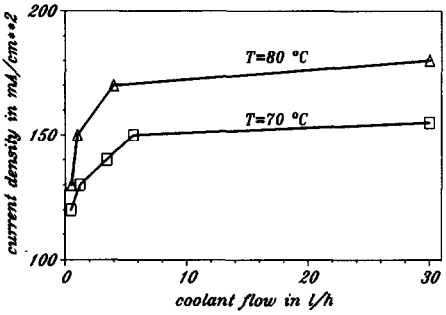

Fig. 8. Isothermal curves in the current density vs. coolant flow diagram.

at the hydrogen twin electrode. This result is important regarding the avoidance of excess degradation of the electrodes during malfunction.

Experience on fuel cell technique is gained by performing detailed parametric investigations. Exemplarly the interrelation between current density, coolant flow and cell temperature has been examined. The results of these calculations are given in Fig. 8 represented by the isothermal lines of the hydrogen twin electrode. Excess heat generation due to increasing current densities cannot be compensated by an increasing coolant flow, indicated by the flat slope of the current density versus coolant flow curve. We conclude that a fuel cell designed for high current densities requires a high efficient cooling system.

From Fig. 8 we also conclude that the optimized operation point regarding the assumed limiting condition is determined by $i = 150$ mA/cm^2 and $\dot{m}_{cool} = 6$ l/h when the stack temperature should not exceed 70 °C.

In addition, minor changes in the modelling program enables the simulation of the thermal performance of advanced fuel cell designs.

Conclusions

A simulation program was developed as a tool to investigate the thermal behavior of hydrogen/oxygen fuel cells in VARTA Eloflux design. This program was used to calculate spatial temperature profiles perpendicular to the electrode surfaces, as well as temperature versus time characteristics. However the temperature distribution parallel to the transversal plane of the cell stack was not considered in the present work. Besides the thermal performance during normal operation, knowledge about the thermal behavior during start-up and operational malfunction has been obtained. These results were used to understand the mechanism of heat rejection and heat dissipation from alkaline fuel cells.

The internal thermal conductivity and heat transition coefficients of each structural component have been calculated on the basis of actual design parameters. The major results are:

- The adjustment of the equilibrium state takes place 2700 s (1500 s within a range of $\Delta T = 3$ K) after start-up operation. This result is important regarding the cyclic operation required for space missions, since this time is in the order of the charge and discharge phases.
- The temperature differences within the electrode stack are predicted to be less than $\Delta T = 5.5$ K for the considered current densities and coolant flows.
- The temperature gradient in the case of malfunction of the cooling system has been determined: $\Delta T/\Delta t = 0.1$ K/s, assuming normal load of the fuel cell.
- Sixty seconds after restarting the coolant flow, readjustment of the equilibrium state takes place within a range of $\Delta T = 3$ K. The occurrence of reentry oscillations is predicted.
- During start-up operation the predicted temperatures were in good agreement with heat rates obtained from integral data, based on the thermoneutral voltage.

The present thermal modelling program could be used to perform detailed parametric investigations required for optimization of the thermal management of alkaline fuel cells. Simulation of certain operation states can be performed by setting the appropriate starting parameters. This program is applicable to fuel cell designs which differ from the present one by minor changes only.

List of symbols

A	area (m^2)
A_{coil}	area of cooling coils (m^2)
A_{El}	electrode area (m^2)
a	thermal conductivity coefficient (m^2/s)
α	heat transition coefficient (W/m^2 K)
c_p	spec. heat capacity (J/kgK)
d	diameter of the pipe (m^2)
i	current density (mA/cm^2)
l	length of pipe (m)
F	Faradays constant (C/mol)
H	enthalpy (J)
λ	heat conductivity (W/mK)
m	mass (kg)
$\dot{m}$	mass flow (kg/s)
$\dot{m}_{cool}$	coolant flow (kg/s)
Nu	Nusselt relation
ν	kinematic viscosity (m^2/s)
Pe	Péclet number
P_r	rated power (W)
Q	heat (J)

Q_{con}	heat flow due to conduction (J/s)
Q_{flow}	heat flow due to mass flow (J/s)
Q_{out}	heat flow out of the fuel cell (J/s)
Q_{in}	heat flow into the fuel cell (J/s)
Q_r	heat flow rejected from the cell (J/s)
Q_{trans}	heat transition (J)
q	heat flow density (J/m^2)
Re	Reynolds number
T	temperature (K)
T_{amb}	ambient temperature (K)
T_{ELO}	temperature of the eloflux flow (K)
T_{KOH}	temperature of the electrolyte (K)
T_{out}	electrolyte temperature at stack output (K)
T_{in}	electrolyte temperature at stack input (K)
U_{fc}	cell voltage (V)
U_0	thermoneutral voltage (V)
W	technical work (J)
w	flow velocity (m/s)
x	distance (m)
z	valence of the ions

References

1 Boeing Aerospace Co., Analysis of regenerative fuel cells, *NASA contract NAS9-16151*, 1982.
2 DLR, Solardynamische Energieversorgungssysteme, *BMFT contract 8603/8*, 1987.
3 A. Levy, L. L. Van Dine and J. K. Stedman, *NASA Rep. No. NASA CR-179609*, 1987.
4 H. Holthusen, *Dissertation*, TU Braunschweig, 1972.
5 A. Winsel and R. Wendtland, *Patent DBP 1546 719* (1965).
6 A. Winsel and R. Wendtland, *Patent DBP 1496 214* (1965).
7 A. Winsel, *Dechema-Monographien, 92* (1982) 21–43.
8 *Gmelins Handbuch der anorganischen Chemie*, Verlag Chemie GmbH, 1953.
9 F. Hell, *Grundlagen der Wärmeübertragung*, VDI-Verlag, 1982.
10 A. Baumann, *Thesis*, University Stuttgart, F.R.G., 1991.